Controlled Removal of Surfactants from Double-Walled Carbon Nanotubes for Stronger *p*-Doping Effect and its Demonstration in Perovskite Solar Cells

Ahmed Shawky,[+] Jeong-Seok Nam,[+] Kyusun Kim,[+] Jiye Han, Jungjin Yoon, Seungju Seo, Chang Soo Lee, Rong Xiang, Yutaka Matsuo, Hyuck Mo Lee, Shigeo Maruyama, Il Jeon**

Dr. A. Shawky, S. Seo, Prof. Y. Matsuo, Prof. R. Xiang, Prof. S. Maruyama
Department of Mechanical Engineering, School of Engineering, The University of Tokyo, Tokyo 113-8656, Japan

J.-S Nam, Dr. K. Kim, J. Han, Prof. I. Jeon,
Department of Chemistry Education, Graduate School of Chemical Materials, Sustainable Utilization of Photovoltaic Energy Research Center, Institute for Plastic Information and Energy Materials, Pusan National University, 63-2 Busandaehak-ro, Busan 46241, Republic of Korea

Dr. J. Yoon,
Department of Materials Science & Engineering, Pennsylvania State University, University Park 16802, PA, United States

Dr. C. Lee, Prof. H. M. Lee,
Department of Materials Science and Engineering, KAIST, 291 Daehak-ro, Yuseong-gu, Daejeon, 34141, Republic of Korea

Prof. Y. Matsuo,
Institute of Materials Innovation, Institutes of Innovation for Future Society, Nagoya University, Furo-cho, Chikusa-ku, Nagoya 464-8603, Japan

E-mail: il.jeon@spc.oxon.org, maruyama@photon.t.u-tokyo.ac.jp,

Double-walled carbon nanotubes have shown the potential as a promising alternative to conventional transparent electrodes owing to solution-processability as well as high conductivity and transparency. However, their DC to optical conductivity ratio is limited by surrounding surfactants preventing *p*-doping of the carbon nanotubes. To maximize the doping effectiveness, the surfactants are removed from double-walled carbon nanotubes with negligible damage to the nanotubes by calcinating in Ar atmosphere. The effective removal of

1

the surfactants was evidenced by various analyses and the results show that 400 °C is the optimal temperature. The conductivity improvement of the double-walled carbon nanotube films by triflic acid increased from 31.9% to 59.7% after the removal of the surfactants. Using the surfactant-removed *p*-doped solution-processed transparent electrodes, inverted-type perovskite solar cells are fabricated and a power conversion efficiency of 17.7% without hysteresis is displayed. This work advances the transparent conductor application of double-walled carbon nanotubes as the efficiency is highest among the reported carbon nanotube electrode-based perovskite solar cells and solution-processable transparent electrode-based solar cells to date.

In the wake of sustainable energy, thin-film photovoltaics have emerged as a promising renewable energy harvester.[1–3] The thin-film photovoltaics have unique advantages of low fabrication cost, solution-processability, and flexibility, all of which other renewable energy technologies do not possess. To maximize these fortes, it is imperative that we replace conventional metal oxide transparent conductors, such as indium tin oxide (ITO),[4–12] which are expensive, inflexible, and limit solution-processability of the thin-film solar cells.[13] In this respect, carbon nanotubes (CNTs) and graphene have been regarded as a suitable alternative to the metal oxide conductors on account of their high dc to optical conductivity ratio and superior mechanical properties.[6,14–17] Among the CNT electrodes, single-walled CNTs have been the most common choice for the transparent electrode application owing to the high transparency arising from low optical density along the tube axis.[18,19] However, neither the single-walled CNTs or graphene can be coated by a solution-process, which still prevents thin-film optoelectronics from being entirely solution-processable. Double-walled CNTs (DWNTs), which sit between single-walled CNTs and multi-walled CNTs, possess high DC to optical conductivity ratio of single-walled CNTs as well as good dispersibility of multi-walled CNTs.[20,21] In our previous study,[22] we

demonstrated DWNT electrode can be solution-processable for optoelectronic applications thanks to the optimum weight-ratios of surfactants.[23,24] Owing to the suitable diameter of 2 – 3 nm[25] and the long tube length, the solution-processed DWNT electrode showed one of the best DC to optical conductivity ratio among the reported solution-processed electrodes.[22] In addition, the solution-processed DWNT-based perovskite solar cells (PSCs) exhibited a power conversion efficiency (PCE) of 17.2%, which was the highest efficiency among the reported solution-processed electrode-based PSCs. While this power output was sufficiently high and comparable to that of conventional ITO-based PSCs, there is room for further improvement as *p*-doping of the DWNTs was limited by the surrounding surfactants. Carboxyl methyl cellulose sodium salt (CMC), which render water-dispersibility to DWNTs by wrapping around DWNTs, prevented dopants from interacting with the DWNTs. Submerging DWNT films in ethanol for a long time could only so much remove the surfactants. Therefore, finding a new method of removing the surfactants from DWNTs without damaging the nanotubes can bring about a breakthrough in the solution-processed DWNT transparent conductor application in optoelectronics.

Hence, we explored ways to remove surfactants from DWNTs by calcination. After testing various conditions, we found that heating the DWNT film at 400 ºC under a constant flow of Ar can effectively remove the surfactants with minor damage to the DWNTs. The untreated DWNT electrodes showed a decrease in sheet resistance by 31.9% on average when chemically doped by triflic acid, whereas the *p*-doping effective was greatly enhanced to 59.7% for the DWNT electrodes from which surfactants were thermally removed. The resulting sheet resistance was as low as 98 Ω sq^{-1} while the transparency was ~87% at the wavelength of 550 nm. The mechanism of the stable removal of the surfactants is studied by various analyses, namely, microscopic equipment, ultraviolet-visible-near infrared (UV-Vis-NIR) absorption and Raman spectroscopy. The potential of the surfactant-removed DWNT films and their device applicability were verified by fabricating PSCs. The surfactant-

removed DWNT electrodes doped by triflic acid were employed in inverted-type PSCs and a PCE of 17.7% was demonstrated. The improved effect of *p*-doping is manifested by the device performance as the PSCs employing pristine DWNT electrodes doped by triflic acid exhibited a PCE of 16.6%. The PCE improvement came chiefly from the difference in fill factor (FF), which were affected by the conductivity of DWNT electrodes. The obtained PCE of 17.7% is the highest efficiency recorded among the reported ITO-free PSCs based on solution-processed electrodes, such as metal nanowire and reduced graphene oxide, as well as dry-transferred CNT electrodes.

DWNT solutions were slot die-coated on glass substrates followed by submerging in ethanol for 24 h to remove as much CMC surfactants as possible. The slot die coated DWNT electrodes were then put to a chemical vapor deposition (CVD) chamber to remove surfactants via thermal treatment under different temperatures either in air or in Ar (**Figure 1a**). CMCs are known to have a melting point of *ca.* 260 °C. and a boiling point of *ca.* 520 °C. Nevertheless, there have been many reports on CMC degrading and sublimating at *ca.* 300 °C during a thermogravimetric analysis (TGA).[26–29] There is also a report that the cellulose component of CMC decomposing at approximately 350 °C.[30] Indeed, our TGA indicates that the CMC powder reduces to carbon fragments at a temperature slightly below 300 °C both in air and in Ar (**Figure 1b**). However, the mass drop rate was slightly greater for the sample in air than the sample in Ar. We suspect the thermal treatment in air removes a somewhat greater amount of CMC owing to oxidation. TGA spectrum of DWNTs without surfactants in air shows that DWNTs start to degenerate via oxidation at 500 °C and disintegrate completely at 600 °C. On the other hand, the mass of DWNTs in Ar does not drop even at high temperatures because there is no oxidation taking place (**Figure 1c**). The fact that the DWNTs are sublimated completely from the boat after TGA in air while the same sample in Ar remained intact confirms this (**Figure S1**). **Figure 1d** shows TGA of the surfactant-wrapped DWNTs in air and Ar. A downslope appears at around 250 °C for both the samples in air and Ar,

indicating the degradation of CMC. The degradation of CMC occurred at a lower temperature for the CMC-wrapped DWNTs than the CMC powder because there is a relatively weaker hydrogen bonding interaction between CMCs when they are used as surfactants for DWNTs (Figure 1b).[31] As predicted from TGA of the DWNT only sample in air, the mass rate of CMC-wrapped DWNTs stayed almost unchanged in Ar. Based on the TGA results, the solution-processed DWNT electrodes were put to a CVD chamber and calcinated at 300 °C, 400 °C and 500 °C for 10 min each under constant flow of Air or Ar (**Figure 2a**). The reason we chose air is because the condition can degenerate a greater amount of the surfactants faster than the Ar atmosphere due to oxidation. However, there is risk of oxidizing DWNTs as well. Inert argon condition may not remove the surfactants as effectively, yet there is less risk of damaging DWNTs. **Figure 2b – 2h** shows the scanning electron microscope (SEM) images of the DWNT films. After the thermal treatment at 300 °C, both of the films in air and in Ar start to show some particles on the DWNT network (**Figure 2c** and **2d**). The more impurities are seen coming off from the DWNTs for the films calcinated at 400 °C (**Figure 2e** and **2f**). We conjecture those impurities to be degenerated CMCs. The films treated at 500 °C show a much-reduced frequency of impurities found on DWNTs which indicates that the components of the surfactants have sublimated in seemingly more effective manner in air than Ar thanks to oxidation (**Figure 2g** and **2h**). Although it is not easy to distinguish, careful observation on the images reveals that the thickness of the individual CNTs are getting thinner for the DWNTs calcinated in Ar over the temperature increase (**Figure 2h** and **S2**). On the contrary, DWNTs thermally treated in air show some areas of the DWNT surface have been etched away (**Figure 2g**). Atomic force microscopy (AFM) was used to assess the morphological change on the DWNT films under different thermal treatment conditions (**Figure S3**). The roughness mean square values (RMS) of the films did not change significantly but the AFM images clearly show that DWNT films calcinated at 400 °C reveal more pronounced individual tubes and bundles, confirming the removal of surfactants. It should be mentioned

that the obtained RMS values mean that the surfactants-removed DWNT electrodes still manifest smooth surface roughness suitable for device application. This is important as the rough surface of previously reported dry-transferred SWNT electrodes exhibit rough surface which undermines open-circuit voltage (V_{OC}) of solar cell devices (**Figure S4** and **Table S1**).

To assess the effect of the removal of the surfactants, we measured the sheet resistance (R_{sheet}) of the DWNT films using the Van der Pauw four probe method. **Table 1** shows that the thermal treatment increased R_{sheet} of the films both in air and in Ar, but more dramatically more in air than in Ar. Oxidation of DWNT in air is suspected to be the reason for this increase. The calcination in Ar, though in much a lesser degree, increased R_{sheet} due possibly to CNTs being damaged by the thermal energy[32,33], or the removal of surfactants might have induced more Schottky CNT junction contacts between DWNTs.[41] To assess the doping effectiveness, we measured R_{sheet} change of the DWNT films after application of triflic acid. By chemically doping DWNTs, R_{sheet} decreased in all cases. The doping effectiveness became greater with the increase in the calcination temperature. This directly proves that the removal of surfactants increases the doping effective but too much of calcination also increases the sheet resistance by thermally damaging the nanotubes. Triflic acid-doped DWNT films calcinated at 400 °C exhibited the lowest R_{sheet} of 129 Ω sq.$^{-1}$. This is a great enhancement in the *p*-doping effective 59.7% compared with the case of pristine DWNT electrodes, which showed a decrease in sheet resistance by 31.9% on average. Despite the doubled doping efficacy by the removal of the surfactants, this is not the full potential effect of the surfactant removal as our computational study shows that the doping effect could be boosted by more than 10 times (**Figure S5** and **Table S2**). We attribute the still limited doping effectiveness to many of the areas where either surfactants or carbon fragments have not been removed. It can also be seen from the transmission electron microscopy (TEM) images of a DWNT film before and after the calcination at 400 °C that the surfactants have greatly reduced from the DWNT network (**Figure S6** and **S7**). However, it appears that a substantial amount of carbon

fragments still remain on the DWNTs. This reveals that quite a significant portion of CMC surfactants turn into carbon fragments without being sublimated, which may also explain the reduced conductivity upon calcination.

Having confirmed that the thermal treatment in Ar removes the surfactants more effectively, the Fourier-transform infrared spectroscopy (FT-IR) was used to ascertain the removal of the surfactants from CMC from DWNTs. **Figure 3a** shows the reduction of a peak at 3500 cm^{-1}, which corresponds to the O-H stretch, indicating the removal or degeneration of CMC upon thermal treatment. However, the C-H stretch at 2900 cm^{-1} remains the same. This comes from the defect sites on DWNTs or carbon fragments surrounding the DWNTs. Unlike FT-IR, the X-ray photoelectron spectroscopy (XPS) measures with a much greater accuracy despite the fact that the penetration depth is *ca.* 5 nm and thereby, it measures the surface of the DWNT film.[34] The intensity of the Na 1s peak, which comes from the CMC on DWNTs increases greatly at the calcination temperature of 300 °C under Ar then decreases rapidly at further elevated calcination temperatures (**Figure 3b**). This trend verifies the CMC coming off the pristine DWNTs to the surface at 300 °C and then sublimating or degenerating at higher temperatures. The O 1s peak intensity, likewise, increases at 300 °C and then decreases back again similar to the trend of the Na 1s peak (**Figure 3c**). It is worth noting that the O 1s peak of DWNTs thermally treated at 300 °C shows a small hump at a lower binding energy, which we is surmised to be from H$_2$O trapped within the DWNT network during the slot die coating.[32,35]

Having seen the evidence for the removal of CMCs from DWNTs, the enhanced doping effectiveness of the surfactant-removed DWNTs was investigated. Visible-near infrared (Vis-NIR) absorption spectroscopy of the DWNTs films calcinated at different temperatures in Ar shows that the van Hove transitions become clearer with an increase in the calcination temperature (**Figure 4a**). Since the CMC surfactant has strong absorption only under 300 nm due probably to lighter scattering only (**Figure S8**), we conjecture that the van

Hove transitions appear due to de-doping of oxygen from DWNTs when calcinated at high temperatures. This might have contributed to the increase in sheet resistance after the calcination (**Table 1**). The suppression of van Hove transition indicates degree of triflic acid-driven *p*-doping. **Figure 4b** shows that the van Hove transitions of the thermally treated DWNT films at 400 °C exhibits greatest suppression even compared with the *p*-doped DWNT films thermally treated at 500 °C. Despite dramatic changes in the absorption in the NIR region, transmittance in the Vis region does not seem to be affected significantly by neither the thermal treatment nor the chemical doping. The high transparency of 87% at 550 nm was retained throughout the treatment (**Figure S9**). The Fermi level shifts measured by the photoelectron yield spectroscopy (PYS) shows that the DWNT films calcinated at 300 °C shows the similar Fermi level of *ca.* 5.1 eV as the reported values of CNT electrodes in general (**Figure S10a**).[22,36–38] Both of the DWNT films calcinated at 400 °C and 500 °C display the lowest Fermi level of ca. 5.41 eV, which is lower than the reported Fermi level of the triflic acid-treated pristine DWNT electrodes (~5.2 eV). The Kelvin probe measurement data show similar trend but the DWNT film calcinated at 500 °C has the lower Fermi level (5.71 eV) than the DWNT film calcinated at 400 °C (5.50 eV) (**Figure S10b**). The discrepancy comes from the similar doping effect the both films have and the difference is not substantial. This matches the results found from the sheet resistance measurement and the Vis-NIR absorption spectroscopy. The Raman spectroscopy under a 532 nm laser was also used to investigate the doping effectiveness of the DWNT films calcinated at different temperatures. The peaks in radial breathing mode (RBM) region between 200 cm^{-1} to 350 cm^{-1} corresponding to the inner tubes of DWNTs becomes much more pronounced for the samples thermally treated at 400 °C and 500 °C (**Figure 4c**).[22,39–41] In addition, while the G band peak position does not change significantly, the intensity ration of the D band over the G band is substantially reduced when the DWNT films were thermally treated (**Figure 4d**).[42] From these results, we can infer that the surfactants are definitely being removed from the

tubes. Upon triflic acid doping, the intensity of the peaks at the RBM region decreased and the degree of decrease was greatest for the DWNT samples calcinated at 500 °C. All of the RBM peaks and the G-band peak shifted to the right upon triflic acid doping (**Figure 4e**).[39,43] However, the shift as well as the intensity ration of the D band over the G band were not significant enough to make distinctions among the DWNT films calcinated at different temperatures (**Figure 4f**).

To confirm the device applicability of the surfactant-removed DWNT transparent electrodes and the enhanced doping effect therein, inverted-type PSCs were fabricated. On a glass substrate DWNT solution was slot die-coated followed by thermal treatment in Ar for 10 min. Subsequently, the DWNT electrodes were *p*-doped by triflic acid according to the method previously reported[22,36,37,44]. The rest of the layers were fabricated in a configuration of DWNT/poly(triaryl amine) (PTAA) [35 nm]/poly[(9,9-bis(30-((N,N-dimethyl)-N-ethylammonium)-propyl)-2,7-fluorene)-alt-2,7-(9,9-dioctylfluorene)] dibromide (PFN-P2) [<10 nm]/$MA_{0.6}FA_{0.4}PbI_{2.9}Br_{0.1}$ [450 nm]/C_{60} [20nm]/bathocuproine (BCP) [6 nm]/Ag [70 nm] (**Figure 5a**). The energy diagram shows that the Fermi level of the triflic acid-doped surfactant-removed DWNT electrodes aligns well with the valence band of the perovskite layer rather than the PTAA layer (**Figure 5b**). On the other hand, the Fermi level of the triflic acid-doped pristine DWNT electrodes aligns well with the valence band of the PTAA layer owing to relatively weak *p*-doping. The photoluminescence (PL) data reveals that perovskite films on the triflic acid-doped surfactant-removed DWNTs show marginally stronger quenching and the blue shifts, meaning that the calcinated DWNTs induce more effective charge transfer (**Figure 5c**). It is interesting that the DWNT calcinated at 500 °C show relatively weaker quenching. All of the devices fabricated exhibited high performance and the difference in the device performance came mainly from fill factor (FF) (**Figure 5e-h** and **Table S2**). However, the difference was not as great as predicted. Expectedly, the series resistance of the devices based on *p*-doped DWNT electrodes calcinated at 400 °C was the

lowest owing to the greatest *p*-doping effect (**Figure 5g** and **Figure S11**). This resulted in the highest FF of 77.2. In the case of the devices based on *p*-doped DWNT electrodes calcinated at 500 °C, FF was similar compared to the devices based on *p*-doped DWNT electrodes calcinated at 300 °C (**Figure 5f** and **5h**). Despite the lower series resistance, the lower shunt resistance arising from the charge recombination led to the similar FF. We suspect the carbon fragments and the thermal damage to the DWNTs during the calcination to be the reason for the low shunt resistance and it is reflected in the PL data in Figure 5c. Even though the enhancement of PCE was not as great as anticipated, the increase in the figure of merit was significant. The *p*-doped DWNT calcinated at 400 °C showed the highest PCE of 17.7% (**Figure 5g** and **Table 2**). The obtained PCE is currently the highest PCE among the reported CNT transparent electrode-based PSCs as far as we are concerned and certainly the highest among the solution-processed transparent electrode-based PSCs (**Table S3** and **Figure S12**).[5,6,22,45–50]

In conclusion, calcinating the solution-processed DWNT electrodes at 400 °C under argon atmosphere effectively removed the surfactants with minimum damage to the nanotubes. The calcination temperature was optimized to avoid thermal damage while maximizing the removal of CMCs. The surfactant-removed DWNTs showed almost doubled effectiveness of *p*-doping when triflic acid was applied. The PSCs fabricated using the solution-processed DWNT electrode with the enhanced doping effect displayed a considerable increase in the PCE. Nonetheless, the increase was not as great as the theoretical prediction of this work. The limitation came from the limited doping effect by the remaining surfactant carbon fragments as well as the inevitable thermal damage to the DWNTs. In addition, the inner-wall of the DWNTs were still protected by the outer-wall. Therefore, finding another method to circumvent the thermal damage as well as imposing strong doping effect on the inner-walls of DWNTs can lead to further advancement of the DWNT electrode research.

Experimental Section

DWNT Synthesis: DWNTs were grown by a catalytic high-temperature chemical vapor deposition. DWNTs were dispersed using a tip-type sonicator (Ieda Trading Corporation, VCX-130) for 45 min at 20 W at carboxyl methyl cellulose sodium salt (Sigma-Aldrich) /DWNTs = 6 (w/w%), then ultra-centrifugated (Hitachi Koki, himac, CP-WX) at 147000 g for 8 h. The top-80% portion of the supernatant was collected, and the sediment was redispersed in water. The sediment/water = 0.04 (w/w%). The DWNT dispersion was diluted in water to 0.04 wt%, which was slot-die coated on large glass substrates, followed by heating at 125 °C for 1 min. The DWNT-coated substrates were submerged in ethanol for 24 h to remove impurities and surfactants.

Surfactant Removal from the DWNT Films: DWNT films were cut into 1.5×1.5 cm^2 pieces and were put into an ultra-high vacuum chamber containing quartz-tube furnace operated at 30 Pa. It was followed by either air or an Ar flow of 300 sccm introduced to the system, and subsequent heating of 300-500 °C for 10 min. The absolute pressure of the chamber increased to 290 Pa. After the process, the chamber was allowed to cool in room temperature while keeping the air or Ar flow.

Device Fabrication: The DWNT substrates were cut to smaller substrates for the fabrication at a lab scale (25×25 mm^2). For Triflic acid doping, 100 μL of triflic acid solution diluted in chlorobenzene (8% v/v) was spin-coated at 4000 rpm for 60 s and the substrate was dried under 130 °C for 30 min. PTAA solution was prepared by dissolving 8 mg of PTAA (Sigma

Aldrich) in 1 mL of 2,3,5,6-tetrafluoro-7,7,8,8-tetracyanoquinodimethane (F4 TCNQ)-added solution which was prepared by dissolving F4 TCNQ into chlorobenzene (Sigma Aldrich) in a concentration of 1 wt%. The PTAA layer was formed by spin-coating the solution on the DWNT substrates with 4000 rpm for 30 s and then annealed on a hotplate at a temperature of 100 °C for 10 min. To secure a reproducible coating of perovskite film on the hydrophobic PTAA layer, PFN-P2 (1-Material) was introduced as an interfacial compatibilizer. Its precursor solution was prepared by dissolving PFN-P2 in methanol with a concentration of 0.4 mg mL^{-1} and spin-coated on the PTAA layer at 4000 rpm for 20 s. Perovskite layer with a composition of $MA_{0.6}FA_{0.4}PbI_{2.9}Br_{0.1}$ was fabricated using a reported method. Perovskite precursor solution was prepared by dissolving 461 mg of PbI_2 (Tokyo Chemical Industry), 79.5 mg of methylammonium iodide (MAI) (Greatcell Solar), 68.8 mg of formamidinium iodide (FAI) (Greatcell Solar), 11.2 mg of methylammonium bromide (MABr) (Greatcell Solar) and 75 μL of the urea-added dimethylsulfoxide (DMSO) (Sigma Aldrich) in 0.55 mL of N-dimethylformamide (DMF) (Sigma Aldrich). The urea solution was prepared by dissolving urea (Sigma Aldrich) in DMSO at a concentration of 44.4 mg mL^{-1} to induce large grain crystallization of perovskite film. The perovskite precursor solution was stirred for 1 hour under room temperature. The solution was spin-coated at 4000 rpm for 20 s. 3~500 μL of diethyl ether antisolvent was applied 7 s after the beginning of the spin-coating. A transparent film of perovskite intermediate phase was formed and changed into a black perovskite film after annealing under a temperature of 130 °C for 20 min. The whole spin-coating process was conducted under the controlled temperature (25 °C) and relative humidity (<10%). Then, C_{60} (20 nm) and BCP (6 nm) layers were deposited through a square metal mask of 1.5×1.5 cm^2 and Ag electrode was deposited to complete devices with an area of 0.3×0.3 cm^2 (0.09 cm^2) under a pressure of $<5.0 \times 10^{-6}$ torr inside a thermal evaporator.

Material and Device Characterization: *J–V* curves of perovskite solar cells under light were measured using a source meter (Keithley 2400, Tektronix) at a step voltage of 20 mV and a delay time of 50 ms for both the forward and reverse scan directions. A metal aperture mask having an area of 0.13×0.58 cm^2 (0.0754 cm^2) was used during the *J–V* measurement. AM 1.5G illumination was simulated using a solar simulator (Solar 3A Class, Oriel) with a KG-5-filtered silicon standard cell. *J–V* curves under dark condition were measured using a probe station built inside a dark-shield box. The van der Pauw method of four probe measurement was conducted using a probe station and indium metal pieces. SEM measurement was conducted using field-emission scanning electron microscopy (Auriga, Carl Zeiss). TEM measurements were conducted using high-resolution scanning/transmission electron microscopy (Talos F200X, FEI and H-7600, Hitachi). For the SEM and TEM measurements, hot-water dipping at 70 °C was used to release the DWNT film from the glass substrates. Then, small Si grids were used to pick the DWNT samples. Optical transmittance and absorption spectra were obtained using a UV-vis-NIR spectrophotometer (Cary 5000, Agilent Technologies). Surface topography measurement was conducted using an atomic force microscope (NX10, Park Systems) via non-contact mode. LUMOS II Stand-Alone FT-IR microscope was used for the FT-IR analysis. EQE spectra were obtained using a quantum efficiency system (IQE-200B, Oriel) with a chopper frequency of 100 Hz. Core-level photoemission measurements were performed by XPS (PerkinElmer, 5400MC) using monochromatic Al Ka radiation. XPS resolution was estimated to be 1 eV, and the energy offset was calibrated using the surface C 1s peak. A Raman microscope with a × 50 lens and 5 × 10^{-6}% of 200 mW power (Renishaw InVia with 532 nm excitation) was used. For the theoretical study, GGA-level spin-polarized DFT calculation was performed as implemented in Vienna ab initio simulation (VASP) package code with a plane wave basis-set. The exchange-correlation energy was described with the Perdew-Burke-Ernzerhof (PBE)[51] functional. The Brillouin zone was sampled with a $1 \times 1 \times 2$ k-point mesh following the

Monkhorst−Pack scheme. The convergence criteria for electronic and geometric optimization were 10^{-4} eV and 0.01 eV Å^{-1}, respectively. The cut-off energy was set to 400 eV. The structure configurations of DWNTs were constructed as described in the previous study.[52] The isolated DWNT were geometrically optimized through fully relaxing the atomic structure. Bader charge analysis[53] was performed for the charge transfer between the dopants and DWNTs.

Supporting Information
Supporting Information is available from the Wiley Online Library or from the author.

References

[1]   Y. Rong, Y. Hu, A. Mei, H. Tan, M. I. Saidaminov, S. Il Seok, M. D. McGehee, E. H. Sargent, H. Han, *Science (80-.).* **2018**, *361*, eaat8235.

[2]   J. Xu, C. C. Boyd, Z. J. Yu, A. F. Palmstrom, D. J. Witter, B. W. Larson, R. M. France, J. Werner, S. P. Harvey, E. J. Wolf, W. Weigand, S. Manzoor, M. F. A. M. van Hest, J. J. Berry, J. M. Luther, Z. C. Holman, M. D. McGehee, *Science (80-.).* **2020**, *367*, 1097.

[3]   M. Graetzel, R. A. J. Janssen, D. B. Mitzi, E. H. Sargent, *Nature* **2012**, *488*, 304.

[4]   A. Kumar, C. Zhou, *ACS Nano* **2010**, *4*, 11.

[5]   I. Jeon, T. Chiba, C. Delacou, Y. Guo, A. Kaskela, O. Reynaud, E. I. Kauppinen, S. Maruyama, Y. Matsuo, *Nano Lett.* **2015**, *15*, 6665.

[6]   I. Jeon, J. Yoon, N. Ahn, M. Atwa, C. Delacou, A. Anisimov, E. I. Kauppinen, M. Choi, S. Maruyama, Y. Matsuo, *J. Phys. Chem. Lett.* **2017**, *8*, 5395.

[7]   H. Park, S. Chang, J. Jean, J. J. Cheng, P. T. Araujo, M. Wang, M. G. Bawendi, M. S. Dresselhaus, V. Bulović, J. Kong, S. Gradečak, *Nano Lett.* **2013**, *13*, 233.

[8]   H. Park, S. Chang, X. Zhou, J. Kong, T. Palacios, S. Gradečak, *Nano Lett.* **2014**, *14*, 5148.

[9]   H. Park, J. Kong, *Adv. Energy Mater.* **2014**, *4*, 1301280.

[10]   I. Jeon, K. Cui, T. Chiba, A. Anisimov, A. G. Nasibulin, E. I. Kauppinen, S. Maruyama, Y. Matsuo, *J. Am. Chem. Soc.* **2015**, *137*, 7982.

[11]   G. Lee, M. Kim, Y. W. Choi, N. Ahn, J. Jang, J. Yoon, S. M. Kim, J.-G. Lee, D. Kang, H. S. Jung, M. Choi, *Energy Environ. Sci.* **2019**, *12*, 3182.

[12]   J. Yoon, H. Sung, G. Lee, W. Cho, N. Ahn, H. S. Jung, M. Choi, *Energy Environ. Sci.* **2017**, *10*, 337.

[13]   S.-H. Bae, H. Zhao, Y.-T. Hsieh, L. Zuo, N. De Marco, Y. S. Rim, G. Li, Y. Yang, *Chem* **2016**, *1*, 197.

[14]   S. Iijima, T. Ichihashi, *Nature* **1993**, *363*, 603.

[15]   S. Iijima, C. Brabec, A. Maiti, J. Bernholc, *J. Chem. Phys.* **1996**, *104*, 2089.

[16]   W. H. Lee, J. Park, S. H. Sim, S. B. Jo, K. S. Kim, B. H. Hong, K. Cho, *Adv. Mater.* **2011**, *23*, 1752.

[17]   H. Park, P. R. Brown, V. Bulović, J. Kong, *Nano Lett.* **2012**, *12*, 133.

[18]   I. Jeon, R. Xiang, A. Shawky, Y. Matsuo, S. Maruyama, *Adv. Energy Mater.* **2019**, *9*, 1801312.

[19]   I. Jeon, Y. Matsuo, S. Maruyama, *Top. Curr. Chem.* **2018**, *376*, 4.

[20]   M. Endo, H. Muramatsu, T. Hayashi, Y. A. Kim, M. Terrones, M. S. Dresselhaus, *Nature* **2005**, *433*, 476.

[21]   Z. Li, H. R. Kandel, E. Dervishi, V. Saini, A. S. Biris, A. R. Biris, D. Lupu, *Appl. Phys. Lett.* **2007**, *91*, 053115.

[22]   I. Jeon, J. Yoon, U. Kim, C. Lee, R. Xiang, A. Shawky, J. Xi, J. Byeon, H. M. Lee, M. Choi, S. Maruyama, Y. Matsuo, *Adv. Energy Mater.* **2019**, *9*, 1901204.

[23]   A. A. Green, M. C. Hersam, *Nat. Nanotechnol.* **2009**, *4*, 64.

[24]   T. Hasan, Z. Sun, P. Tan, D. Popa, E. Flahaut, E. J. R. Kelleher, F. Bonaccorso, F. Wang, Z. Jiang, F. Torrisi, G. Privitera, V. Nicolosi, A. C. Ferrari, *ACS Nano* **2014**, *8*, 4836.

[25]   N. Imazu, T. Fujigaya, N. Nakashima, *Sci. Technol. Adv. Mater.* **2014**, *15*, 025005.

[26]   L. Golbaghi, M. Khamforoush, T. Hatami, *Carbohydr. Polym.* **2017**, *174*, 780.

[27]   A. Pettignano, A. Charlot, E. Fleury, *Polymers (Basel).* **2019**, *11*, 1227.

[28]   A. A. Ibrahim, A. M. Adel, Z. H. A. El–Wahab, M. T. Al–Shemy, *Carbohydr. Polym.* **2011**, *83*, 94.

[29]   T. Sugama, T. Pyatina, *Cem. Concr. Compos.* **2015**, *55*, 281.

[30]   D. de Britto, O. B. G. Assis, *Thermochim. Acta* **2009**, *494*, 115.

[31]   H.-S. Lin, S. Okawa, Y. Ma, S. Yotsumoto, C. Lee, S. Tan, S. Manzhos, M. Yoshizawa, S. Chiashi, H. M. Lee, T. Tanaka, H. Kataura, I. Jeon, Y. Matsuo, S. Maruyama, *Chem. Mater.* **2020**, *32*, 5125.

[32]   J. V. Rojas, M. Toro-Gonzalez, M. C. Molina-Higgins, C. E. Castano, *Mater. Sci. Eng. B* **2016**, *205*, 28.

[33]   D. Priftis, G. Sakellariou, D. Baskaran, J. W. Mays, N. Hadjichristidis, *Soft Matter* **2009**, *5*, 4272.

[34]   I. Jeon, S. Nakao, Y. Hirose, T. Hasegawa, Y. Matsuo, *Adv. Electron. Mater.* **2016**, *2*, 1500341.

[35]   M. Biswas, Y. S. Jung, H. K. Kim, K. Kumar, G. J. Hughes, S. Newcomb, M. O. Henry, E. McGlynn, *Phys. Rev. B* **2011**, *83*, 235320.

[36] Y. Qian, I. Jeon, Y. Ho, C. Lee, S. Jeong, C. Delacou, S. Seo, A. Anisimov, E. I. Kaupinnen, Y. Matsuo, Y. Kang, H. Lee, D. Kim, J. Delaunay, S. Maruyama, *Adv. Energy Mater.* **2020**, *10*, 1902389.

[37] I. Jeon, C. Delacou, H. Okada, G. E. Morse, T.-H. Han, Y. Sato, A. Anisimov, K. Suenaga, E. I. Kauppinen, S. Maruyama, Y. Matsuo, *J. Mater. Chem. A* **2018**, *6*, 14553.

[38] I. Jeon, A. Shawky, S. Seo, Y. Qian, A. Anisimov, E. I. Kauppinen, Y. Matsuo, S. Maruyama, *J. Mater. Chem. A* **2020**, *8*, 11141.

[39] F. Villalpando-Paez, H. Son, S. G. Chou, G. G. Samsonidze, Y. A. Kim, H. Muramatsu, T. Hayashi, M. Endo, M. Terrones, M. S. Dresselhaus, *Phys. Rev. B* **2009**, *80*, 035419.

[40] M. S. Dresselhaus, G. Dresselhaus, R. Saito, A. Jorio, *Phys. Rep.* **2005**, *409*, 47.

[41] A. Jorio, C. Fantini, M. A. Pimenta, R. B. Capaz, G. G. Samsonidze, G. Dresselhaus, M. S. Dresselhaus, J. Jiang, N. Kobayashi, A. Grüneis, R. Saito, *Phys. Rev. B* **2005**, *71*, 075401.

[42] L. Shi, M. Sauer, O. Domanov, P. Rohringer, P. Ayala, T. Pichler, *Phys. status solidi* **2015**, *252*, 2558.

[43] E. B. Barros, H. Son, G. G. Samsonidze, A. G. Souza Filho, R. Saito, Y. A. Kim, H. Muramatsu, T. Hayashi, M. Endo, J. Kong, M. S. Dresselhaus, *Phys. Rev. B* **2007**, *76*, 045425.

[44] T.-H. Han, S.-J. Kwon, N. Li, H.-K. Seo, W. Xu, K. S. Kim, T.-W. Lee, *Angew. Chemie Int. Ed.* **2016**, *55*, 6197.

[45] I. Jeon, S. Seo, Y. Sato, C. Delacou, A. Anisimov, K. Suenaga, E. I. Kauppinen, S. Maruyama, Y. Matsuo, *J. Phys. Chem. C* **2017**, *121*, 25743.

[46] H. Chen, M. Li, X. Wen, Y. Yang, D. He, W. Choy, H. Lu, *Nanomaterials* **2019**, *9*, 193.

[47] S. Kang, J. Jeong, S. Cho, Y. J. Yoon, S. Park, S. Lim, J. Y. Kim, H. Ko, *J. Mater. Chem. A* **2019**, *7*, 1107.

[48] Y. Jin, Y. Sun, K. Wang, Y. Chen, Z. Liang, Y. Xu, F. Xiao, *Nano Res.* **2018**, *11*, 1998.

[49] E. Lee, J. Ahn, H.-C. Kwon, S. Ma, K. Kim, S. Yun, J. Moon, *Adv. Energy Mater.* **2018**, *8*, 1702182.

[50] J. Han, S. Yuan, L. Liu, X. Qiu, H. Gong, X. Yang, C. Li, Y. Hao, B. Cao, *J. Mater. Chem. A* **2015**, *3*, 5375.

[51] J. P. Perdew, K. Burke, M. Ernzerhof, *Phys. Rev. Lett.* **1996**, *77*, 3865.

[52] S. Peng, K. Cho, *Nano Lett.* **2003**, *3*, 513.

[53] W. Tang, E. Sanville, G. Henkelman, *J. Phys. Condens. Matter* **2009**, *21*, 084204.

[54] I. Jeon, J. Yoon, U. Kim, C. Lee, R. Xiang, A. Shawky, J. Xi, J. Byeon, H. M. Lee, M. Choi, S. Maruyama, Y. Matsuo, *Adv. Energy Mater.* **2019**, *9*, 1901204.
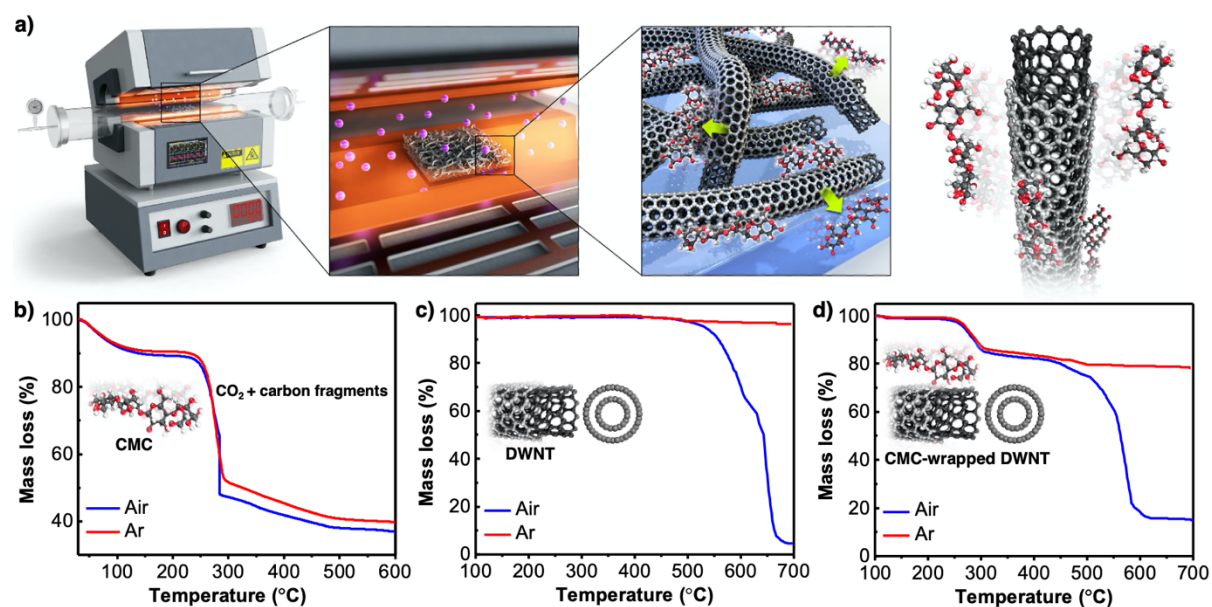
Figure 1. a) Illustration of thermal process under a constant flow of argon effectively removing surfactants from DWNTs. TGA plots for b) CMC surfactant only, c) DWNTs only in Air (red) and in Ar (blue), and d) CMC surfactants-wrapped DWNTs in Air (red) and in Ar (blue).
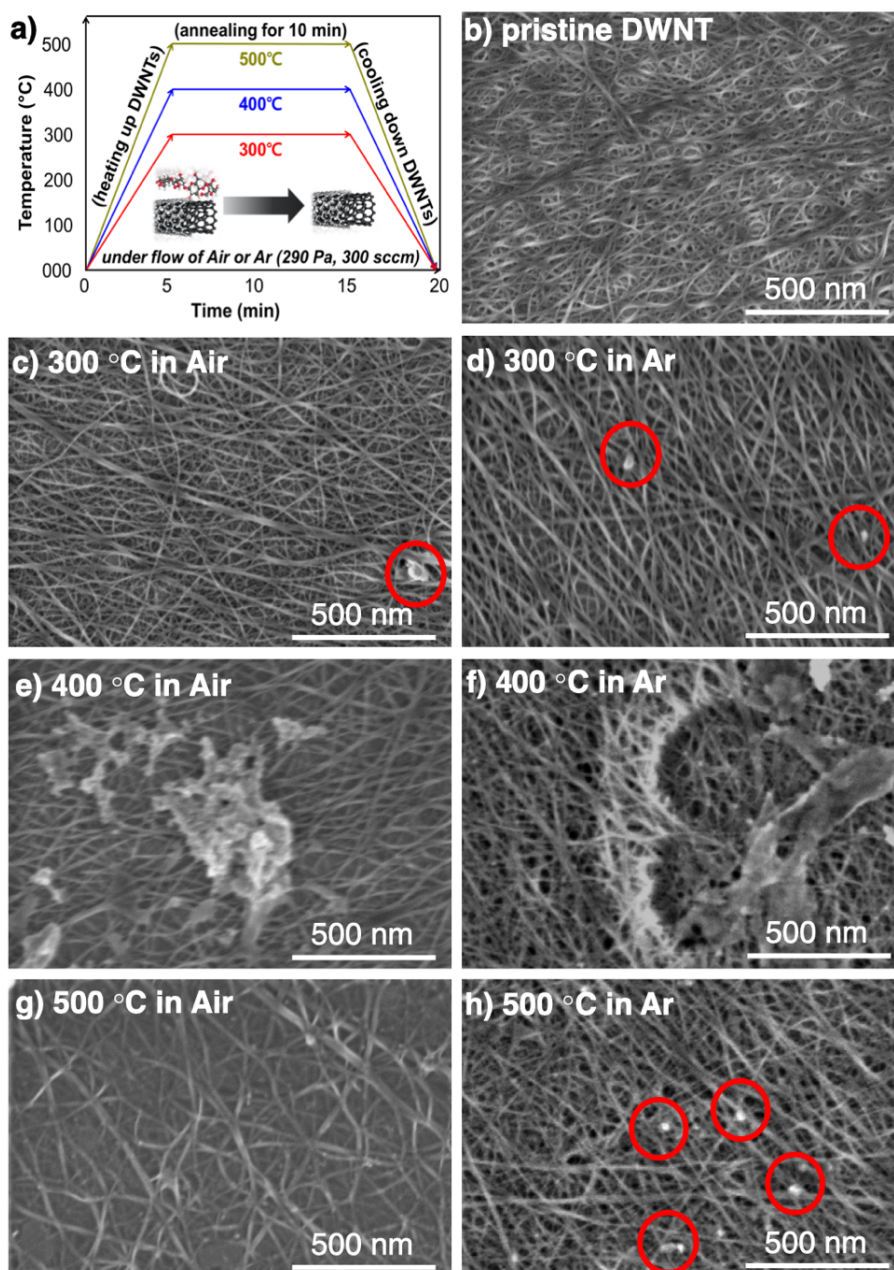
Figure 2. a) Thermal treatment process conducted in this work. SEM images of b) a pristine DWNT film, DWNT films calcinated at 300 °C under c) air and d) Ar, DWNT films calcinated at 400 °C under e) air and f) Ar, and DWNT films calcinated at 500 °C under g) air and h) Ar.
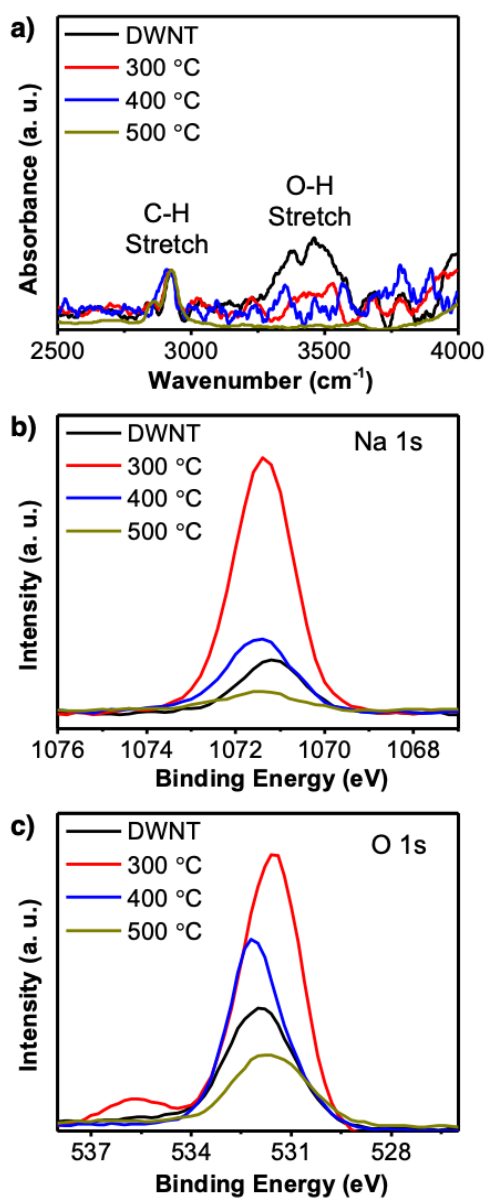
Figure 3. a) FT-IR spectra of a pristine DWNT film (black), a DWNT film calcinated at 300 °C (red), at 400 °C (blue), and at 500 °C (khaki) under Ar atmosphere. XPS spectra of b) Na 1s peak and c) O 1s peak of of a pristine DWNT film (black), a DWNT film calcinated at 300 °C (red), at 400 °C (blue), and at 500 °C (khaki) under Ar atmosphere.
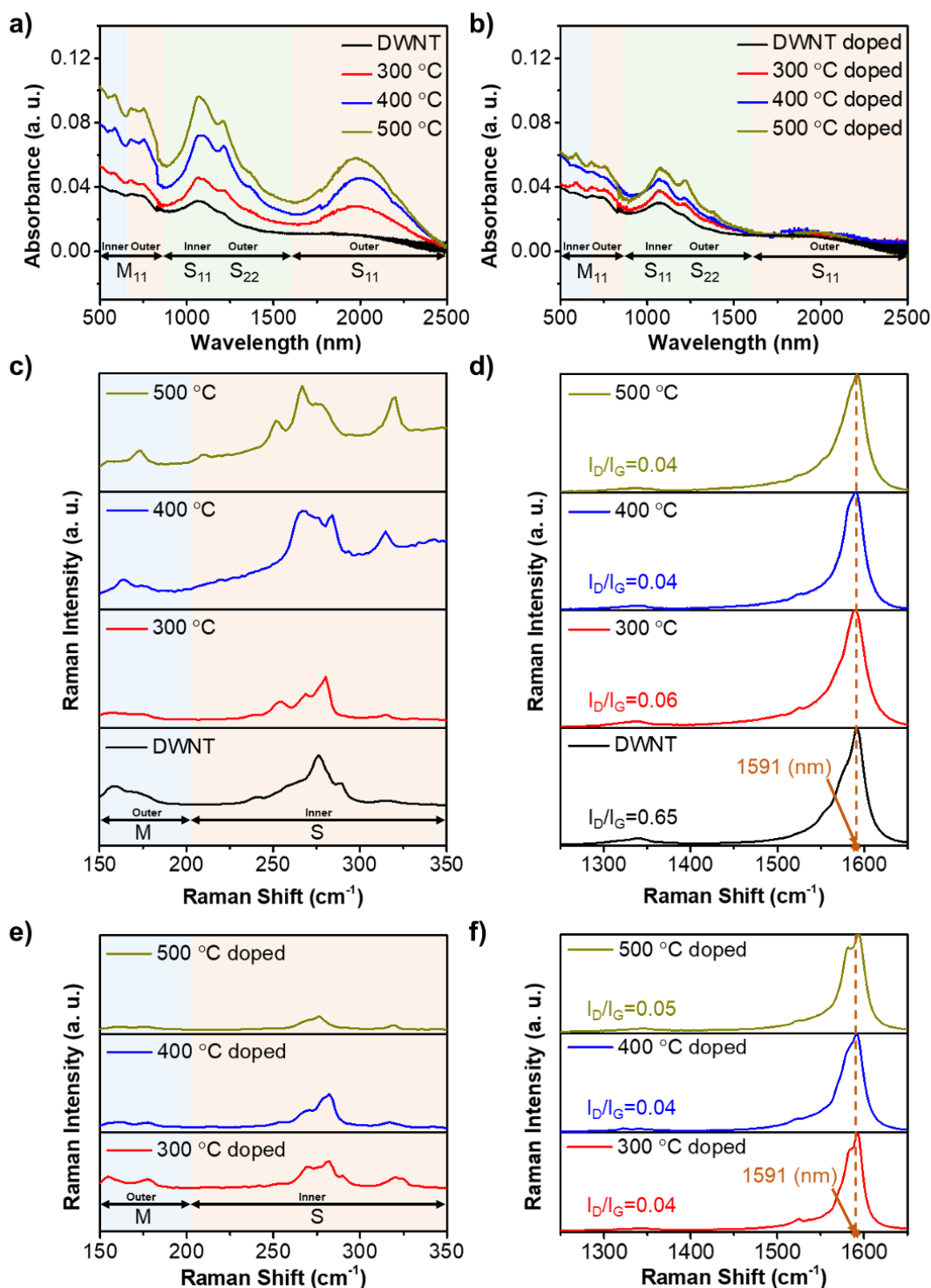
Figure 4. Vis-NIR spectra of a pristine DWNT film (black), a DWNT film calcinated at 300 °C (red), at 400 °C (blue), and at 500 °C (khaki) under Ar atmosphere a) before and b) after triflic acid doping. Raman c) RBM spectra and d) G bands of a pristine DWNT film (black), a DWNT film calcinated at 300 °C (red), at 400 °C (blue), and at 500 °C (khaki) under Ar atmosphere. Raman e) RBM spectra and f) G bands of the same films after triflic acid doping.
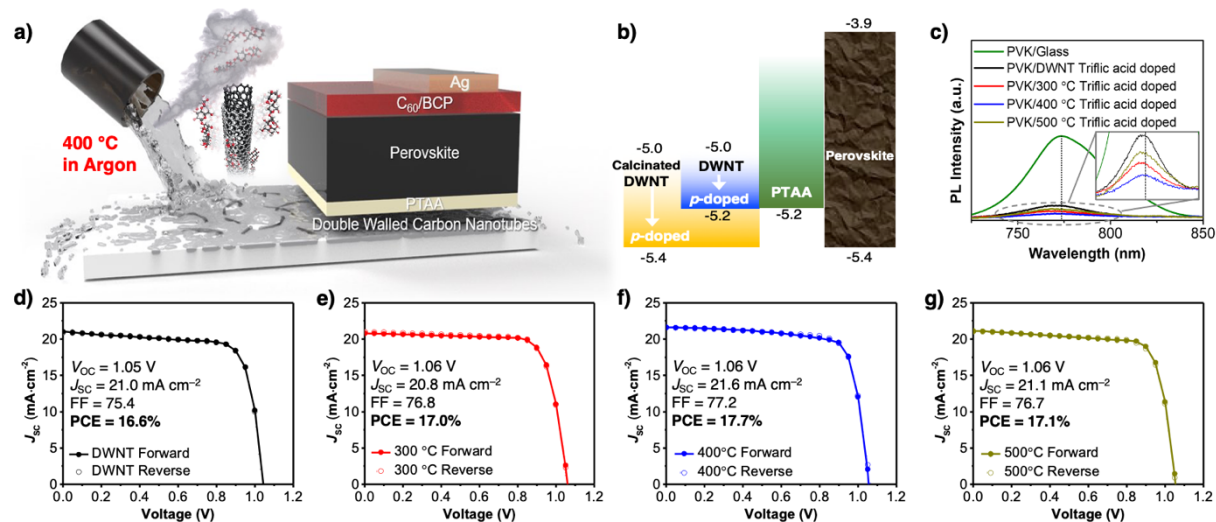
Figure 5. a) 3D illustration of the calcinated DWNT transparent electrode in a PSC device. b) Energy diagram of the DWNT/PTAA/perovskite film interface. c) PL quenching of the perovskite film (PVK) on triflic acid-doped pristine DWNT (black), on triflic acid-doped 300 °C-calcinated DWNT (red), on triflic acid-doped 400°C-calcinated DWNT (blue), and on triflic acid-doped 500 °C-calcinated DWNT (khaki). $J–V$ forward and reverse bias curves measured under AM 1.5G one-sun illumination and the corresponding photovoltaic parameters of the PSCs based on d) triflic acid-doped pristine DWNT, e) triflic acid-doped 300 °C-calcinated DWNT, f) triflic acid-doped 400 °C-calcinated DWNT, and g) triflic acid-doped 500 °C-calcinated DWNT.

Table 1. R_{sheet} of the pristine and the surfactant-calcinated DWNT films in air and Ar before and after p-doping by triflic acid. 10 samples were measured for each measurement.

Calcination Tempt.	Sheet resistance after CVD in Air (Ω sq^{-1})		Sheet resistance after CVD in Ar (Ω sq^{-1})	
	undoped	doped	undoped	doped
Pristine	276 ±29 (before doping) → 188 ±42 (after doping)			
300 °C	370 ±43	216 ±39	299 ±37	201 ±69
400 °C	607 ±78	418 ±92	320 ±63	129 ±30
500 °C	2584 ±211	1196 ±341	414 ±59	198 ±28

Table 2. Average and best photovoltaic parameter values of the triflic acid-doped surfactant-removed DWNT-based PSCs under AM 1.5G one-sun illumination.

Anode		V_{OC} (V)	J_{SC} (mA cm^{-2})	FF	PCE (%)
pristine DWNT	Average	0.05 ±0.01	20.9 ±0.7	75.1 ±0.9	16.4 ±0.7
	Best	1.05	21.0	75.4	16.6
300 °C-calcinated DWNT	Average	1.05 ±0.01	20.0 ±0.9	76.7 ±0.2	16.9 ±0.1
	Best	1.06	20.8	76.8	17.0
400 °C-calcinated DWNT	Average	1.06 ±0.00	21.0 ±0.9	77.0 ±0.4	17.6 ±0.3
	Best	1.06	21.6	77.2	17.7
500 °C-calcinated DWNT	Average	1.06 ±0.00	21.0 ±1.0	76.0 ±0.4	17.0 ±0.2
	Best	1.06	21.1	76.7	17.1

Surfactant-removal from solution-processed double-walled carbon nanotube film by thermal treatment in argon atmosphere enables strong chemical *p*-doping. Calcinating the double-walled carbon nanotubes at 400 °C for 10 minutes under a constant flow of argon effectively removes the surfactants with minimal damage to the nanotubes, increasing the doping effectiveness from 31.9% to 59.7%. The enhanced *p*-doping effect is reflected by transparent conductor application in perovskite solar cells and an efficiency increase from 16.6% to 17.7% is exhibited.

Keywords: Double-walled nanotubes, Surfactant removal, Transparent electrode, Doping effect, Indium-free, Perovskite solar cells

A. Shawky, J.-S. Nam, K. Kim, J. Han, J. Yoon, S. Seo, C. S. Lee, R. Xiang, Y. Matsuo, H. M. Lee, S. Maruyama*, I. Jeon*

Controlled Removal of Surfactants from Double-Walled Carbon Nanotubes for Stronger *p*-Doping Effect and its Demonstration in Perovskite Solar Cells
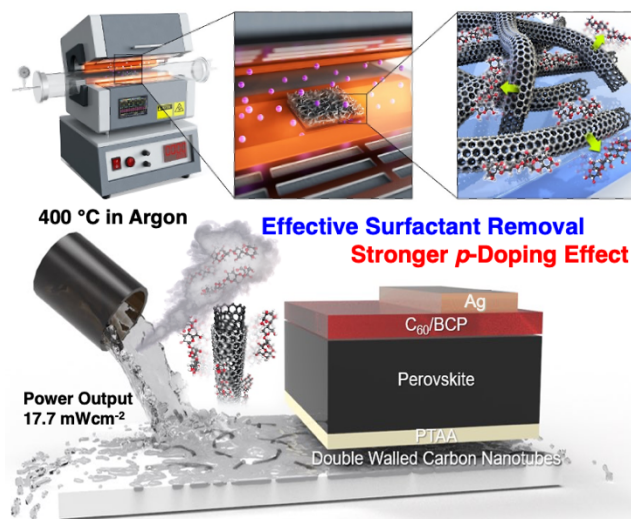
Supporting Information

Controlled Removal of Surfactants from Double-Walled Carbon Nanotubes for Stronger *p*-Doping Effect and its Demonstration in Perovskite Solar Cells

Ahmed Shawky,[+] Jeong-Seok Nam,[+] Kyusun Kim,[+] Jiye Han, Jungjin Yoon, Seungju Seo, Chang Soo Lee, Rong Xiang, Yutaka Matsuo, Hyuck Mo Lee, Shigeo Maruyama*, Il Jeon*
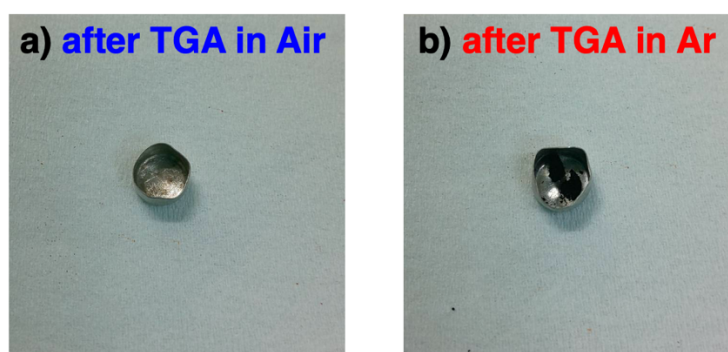
Figure S1. DWNTs inside a boat after TGA in a) air and b) Ar.
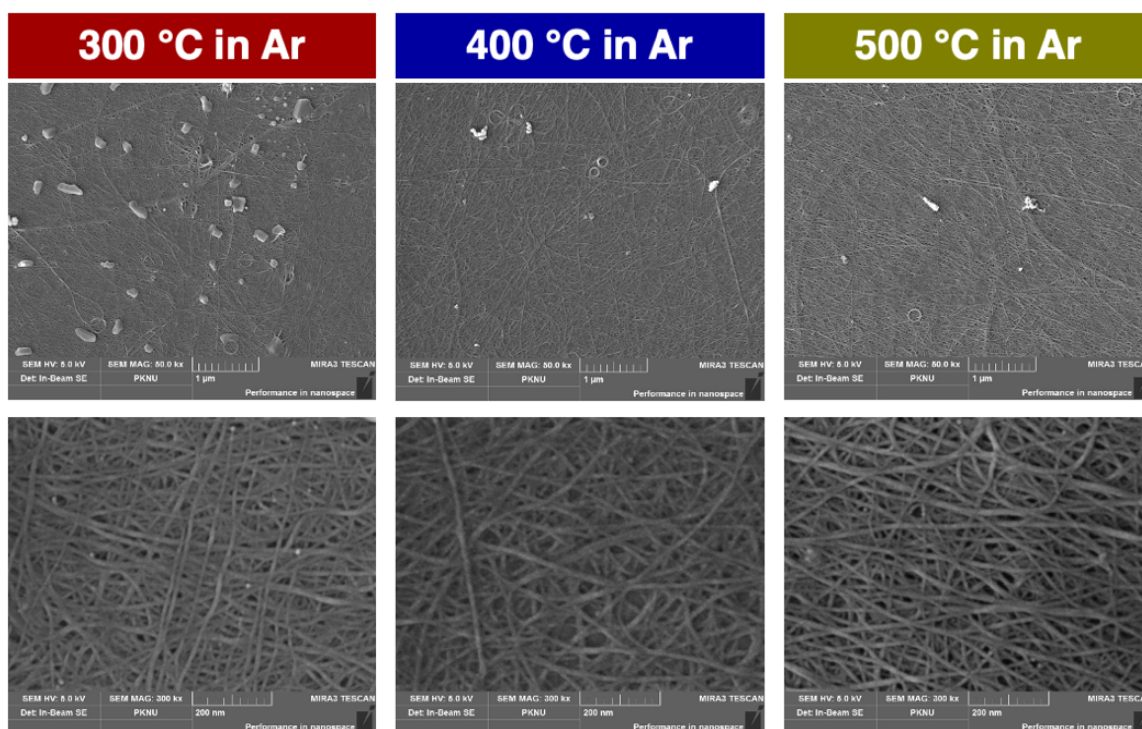

Figure S2. Additional SEM images of DWNT films thermally treated in Ar.
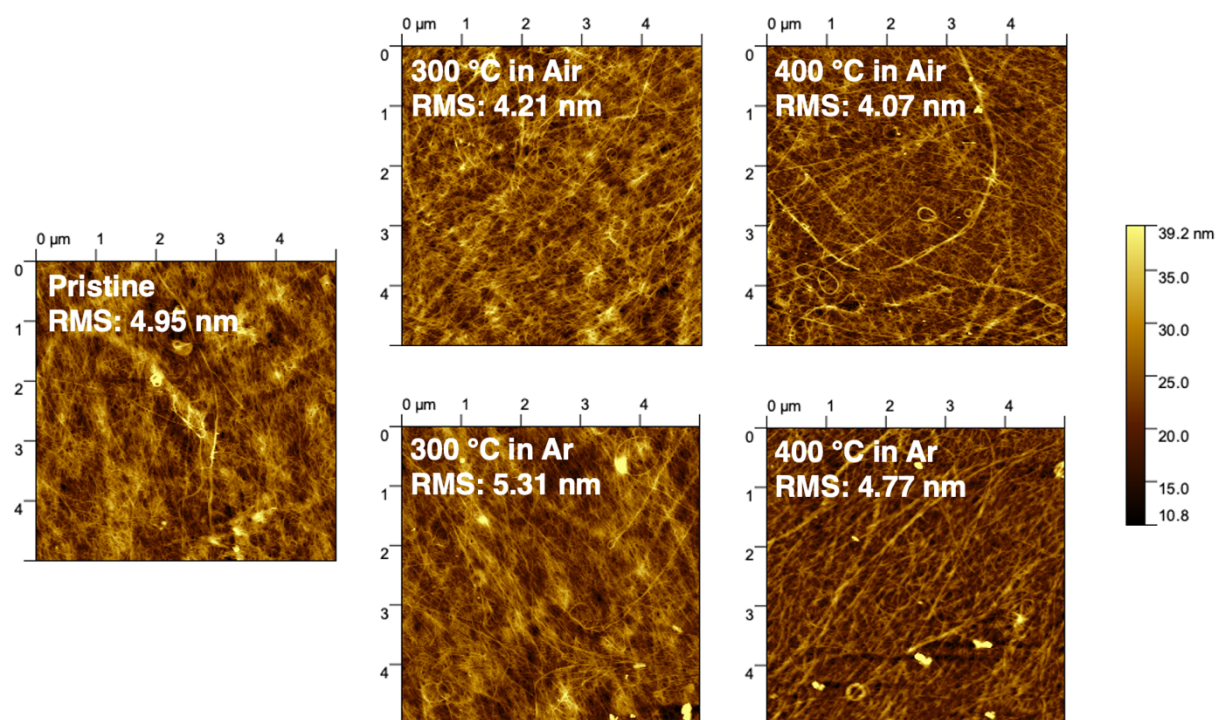
Figure S3. AFM images and RMS values of DWNT films thermally treated at different temperatures in air and Ar.

Table S1. Previously reported V_{OC} and the roughness of carbon electrodes.

Electrode	Charge selection layer	Solar cell type	Reported V_{OC} (V)	Reference no.
HNO$_3$-doped SWNT	PEDOT:PSS[a]	Perovskite	0.79	[5]
ITO			0.83	
MoO$_x$-doped SWNT	PEDOT:PSS	Perovskite	0.90	[6]
MoO$_x$-doped graphene			0.97	
ITO			0.96	
MoO$_x$-doped SWNT	PEDOT:PSS	Organic	0.72	[10]
ITO			0.74	
Polymer-doped SWNT	MoO$_3$	Organic	0.80	[37]
ITO			0.81	
HNO$_3$-doped SWNT	PEDOT:PSS	Perovskite	0.81	[45]
ITO			0.93	
HNO$_3$-doped DWNT	PTAA	Perovskite	1.01	[54]
ITO			1.06	

a: PEDOT:PSS = poly(3,4-ethylenedioxythiophene)
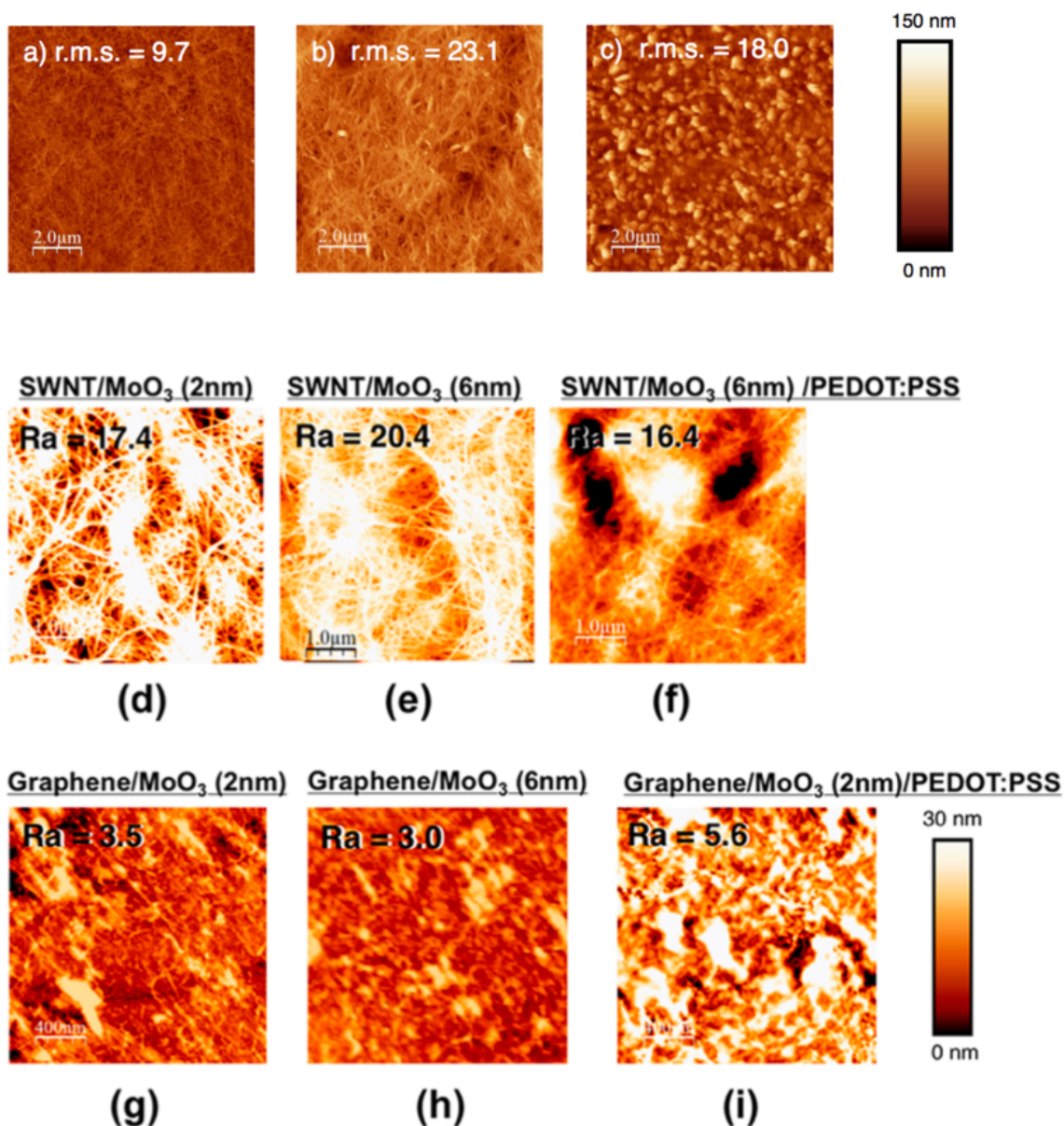
Figure S4. AFM images with RMS roughness values of a) a SWNT film, b) a SWNT film with MoO$_x$ on top, and c) a SWNT film with MoO$_x$ and PEDOT:PSS. Reproduced with permission[10] Copyright 2015, American Chemical Society. AFM images with average roughness (Ra) values of d) a SWNT film, e) a 6nm-thick MoO$_3$-deposited SWNT film, f) a 6nm-thick MoO$_3$-deposited SWNT film with a PEDOT:PSS overcoat, g) a graphene film, h) a graphene film with 2 nm-thick MoO$_3$, and i) a 2 nm-thick MoO$_3$-deposited graphene with a PEDOT:PSS overcoat. Reproduced with permission[6] Copyright 2017, American Chemical Society.
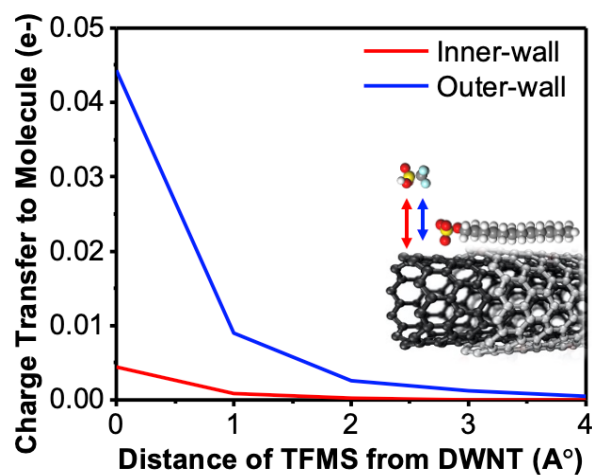
Figure S5. DFT-calculated binding energy between a DWNT and a dopant as the distance increases for triflic acid.

Table S2. Charge transfer between a DWNT and a triflic acid over distance using the Bader charge analysis.

Charge transfer per molecule[a]	Outer-wall of DWNT		Inner-wall of DWNT	
Distance between DWNT and triflic acid (Å)	Zigzag	Armchair	Zigzag	Armchair
0	+0.0379 e⁻	+0.0508 e⁻	+0.0037 e⁻	+0.0050 e⁻
1	+0.0073 e⁻	+0.0106 e⁻	+0.0007 e⁻	+0.0010 e⁻
2	+0.0021 e⁻	+0.0031 e⁻	+0.0002 e⁻	+0.0003 e⁻
3	+0.0010 e⁻	+0.0015 e⁻	+0.0000 e⁻	+0.0000 e⁻
4	+0.0004 e⁻	+0.0005 e⁻	+0.0000 e⁻	+0.0000 e⁻

a: The calculated charge transfer value is small, because it was calculated in a closed system. An actual environment will be an open system, in which the charge transfer value will be much greater.
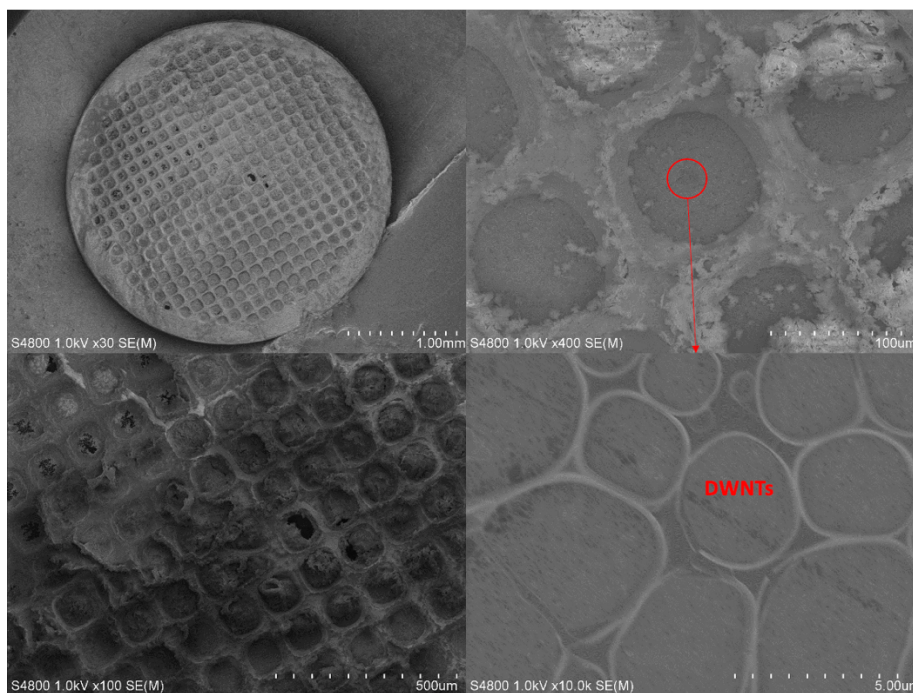
Figure S6. SEM images showing how the DWNT film sampling was done for the TEM measurement.
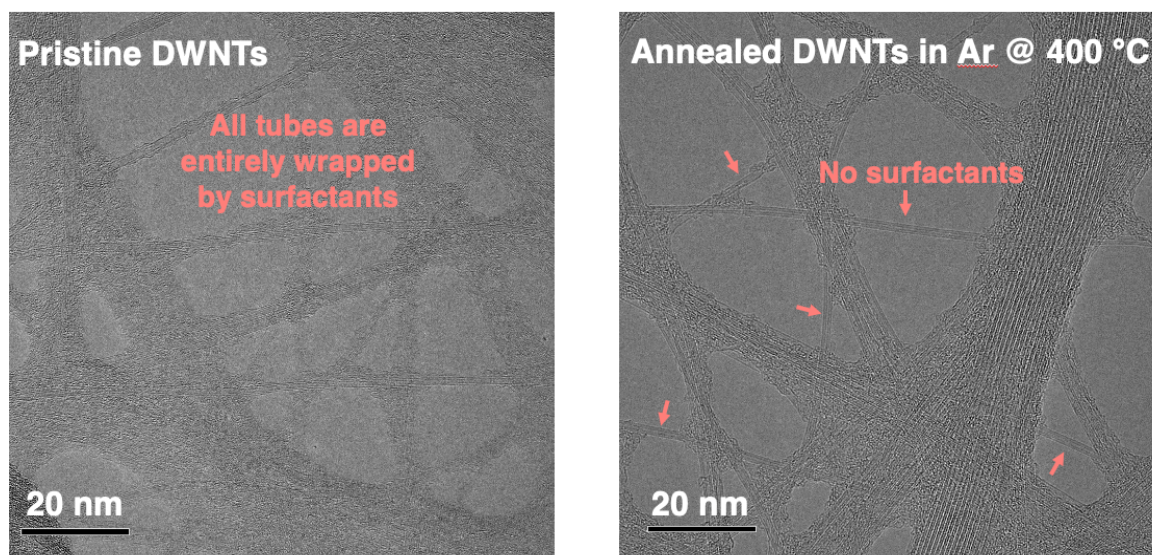
Figure S7. TEM images of a pristine DWNT film (left) and a 400 °C-calcinated DWNT film (right).
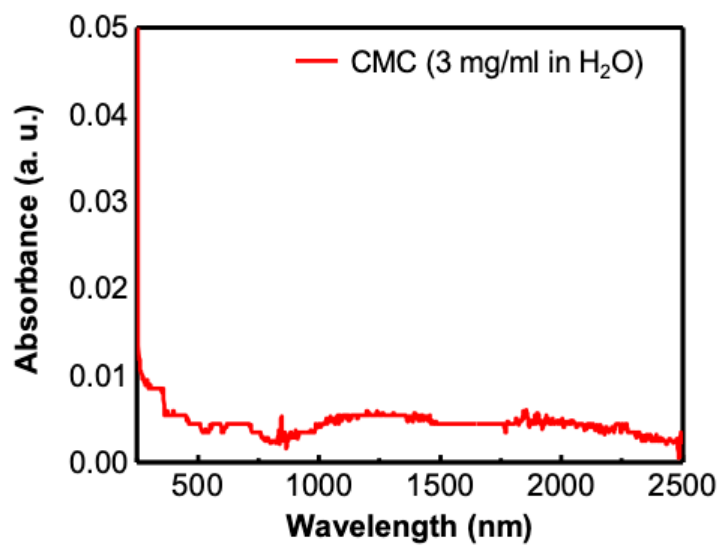
Figure S8. Vis-NIR absorption spectrum of CMCs in water
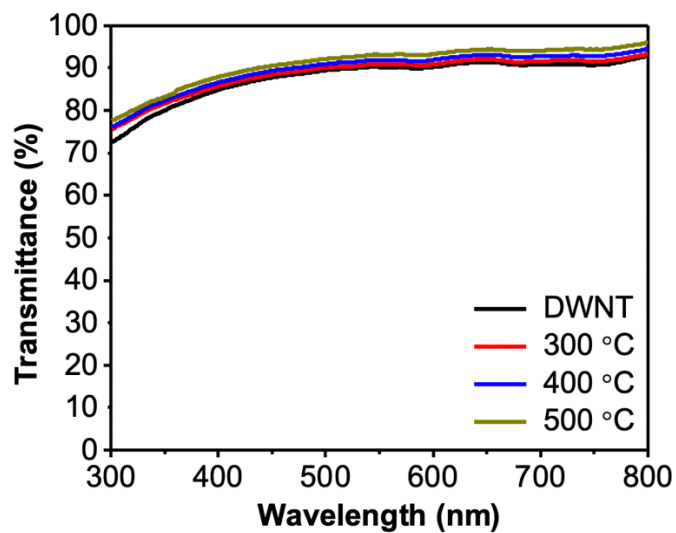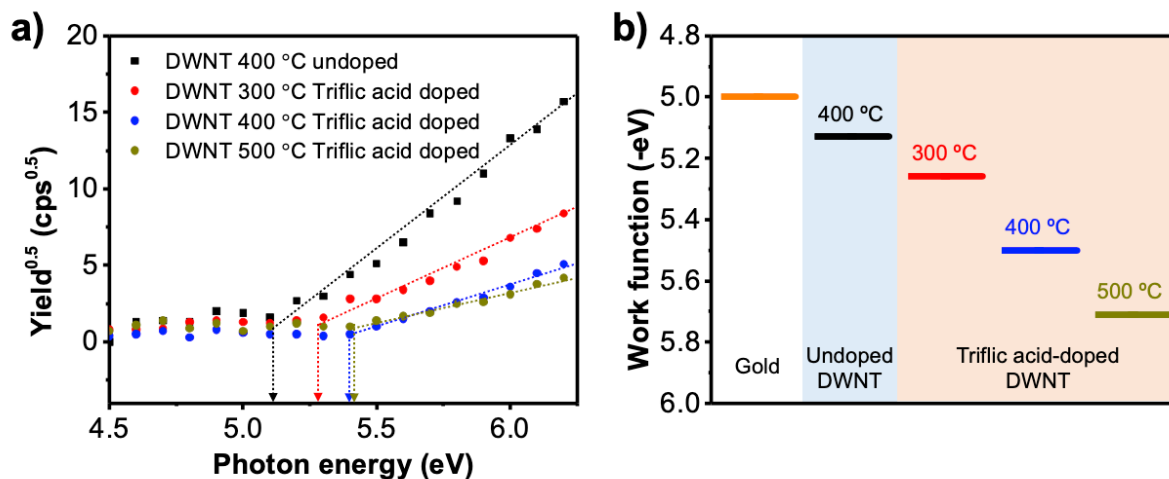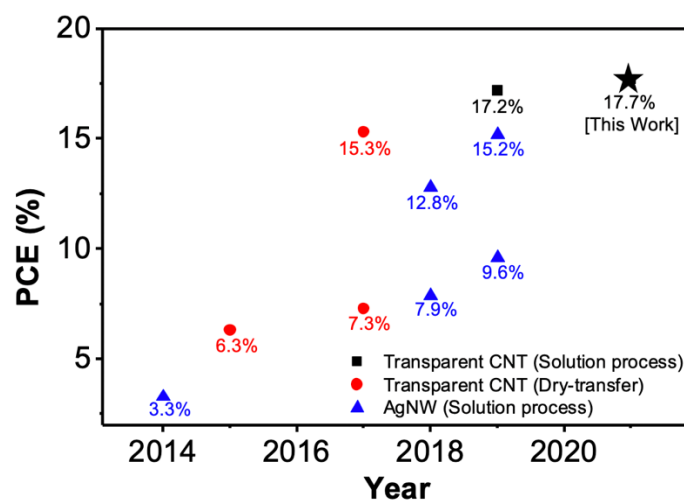

Figure S9. Vis-NIR transmittance spectra of the pristine and calcinated DWNT films

Figure S10. a) PYS measurement of a calcinated DWNT film at 300 °C (black square), triflic acid-doped calcinated DWNT at 300 °C (red circles), at 400 °C (blue circles), and at 500 °C (khaki circles). b) Illustration of the Kelvin-probe measured Fermi levels of the DWNT films.

Figure S11.

Figure S12. Record chart of the reported PCEs of the CNT transparent electrode-based and the solution-processed transparent electrode-based PSCs. AgNW is silver nanowire.

Table S3. Table containing the reported photovoltaic performance and electrode information of the CNT transparent electrode-based as well as the solution-processed transparent electrode-based PSCs.

Year	Bottom Electrode Type	Deposition Technique	PCE (%)	Reference
2021	**triflic acid-DWNT**	**Solution (Slot die-coating)**	**17.7**	**This Work**
2019	triflic acid-DWNT	Solution (Slot die-coating)	17.2	[22]
2019	HNO$_3$-DWNT	Solution (Slot die-coating)	16.7	
2017	HNO$_3$-SWNT	Dry transfer	15.3	[6]
2017	P3HT-CNT	Dry transfer	7.3	[45]
2015	HNO$_3$-SWNT	Dry transfer	6.32	[5]
2019	AgNW/RLGO	Solution (Spin-coating)	9.62	[46]
2019	orthogonal AgNW	Solution (Capillary printing)	15.18	[47]
2018	AgNW/Chi-AsA	Solution	7.88	[48]
2018	a-AZO/AgNW/AZO	Solution (Spin-coating)	12.8	[49]
2015	AgNW/FZO	Solution (Spin-coating) + ALD	3.29	[50]